

This work has been submitted to the IEEE for possible publication. Copyright may be transferred without notice, after which this version may no longer be accessible.

Statistical Analysis and End-to-End Performance Evaluation of Traffic Models for Automotive Data

Marcello Bullo, *Student Member, IEEE*, Amir Ashtari Gargari, Paolo Testolina, *Member, IEEE*, Michele Zorzi, *Fellow, IEEE*, Marco Giordani, *Member, IEEE*

Abstract—Autonomous driving is a major paradigm shift in transportation, with the potential to enhance safety, optimize traffic congestion, and reduce fuel consumption. Although autonomous vehicles rely on advanced sensors and on-board computing systems to navigate without human control, full awareness of the driving environment also requires a cooperative effort via Vehicle-To-Everything (V2X) communication. Specifically, vehicles send and receive sensor perceptions to/from other vehicles to extend perception beyond their own sensing range. However, transmitting large volumes of data can be challenging for current V2X communication technologies, so data compression represents a crucial solution to reduce the message size and link congestion.

In this paper, we present a statistical characterization of automotive data, focusing on Light Detection and Ranging (LiDAR) sensors. Notably, we provide models for the size of both raw and compressed point clouds. The use of statistical traffic models offers several advantages compared to using real data, such as faster simulations, reduced storage requirements, and greater flexibility in the application design. Furthermore, statistical models can be used for understanding traffic patterns and analyzing statistics, which is crucial to design and optimize wireless networks. We validate our statistical models via a Kolmogorov-Smirnoff (KS) test implementing a Bootstrap Resampling scheme. Moreover, we show via ns-3 simulations that using statistical models yields comparable results in terms of latency and throughput compared to real data, which also demonstrates the accuracy of the models.

Index Terms—Automotive data; Vehicle-To-Everything (V2X) communication; statistical modeling; ns-3; KS test.

Marcello Bullo was with the Department of Information Engineering (DEI) of the University of Padova, Italy. He is now with the Department of Electrical and Electronic Engineering, Imperial College London, UK. Email: m.bullo21@imperial.ac.uk.

Amir Ashtari Gargari was with the Department of Information Engineering (DEI) of the University of Padova, Italy. He is now with the Centre Tecnologic de Telecomunicacions de Catalunya (CTTC), Barcelona, Spain. Email: amir.ashtari@cttc.cat.

Paolo Testolina was with the Department of Information Engineering (DEI) of the University of Padova, Italy. He is now with Northeastern University, Boston, MA, USA. Email: p.testolina@northeastern.edu.

Michele Zorzi and Marco Giordani are with the Department of Information Engineering (DEI) of the University of Padova, Italy. Email: {giordani,zorzi}@dei.unipd.it.

This work received funding from UKRI (Grant No. EP/X030806/1), and it was partially supported by the European Union under the Italian National Recovery and Resilience Plan (NRRP) of NextGenerationEU, partnership on “Telecommunications of the Future” (PE0000001 - program “RESTART”). The work of P. Testolina was partially supported by Fondazione CaRiPaRo under grants “Dottorati di Ricerca” 2019.

I. INTRODUCTION

AUTONOMOUS driving is expected to play a critical role in the development of future sixth generation (6G) wireless networks [1], redefining the way we perceive, interact with, and utilize vehicles on the roads. This paradigm will reduce accidents, improve the traffic flow, decrease the fuel consumption, and provide newfound mobility options for individuals with disabilities and older people [2].

Unlike conventional vehicles where a human driver takes control, autonomous vehicles will be equipped with sensors and powerful computing units to perceive the environment, make driving decisions, and navigate autonomously [3]. Besides videocameras, Light Detection and Ranging (LiDAR) sensors are often used, as they are the most precise systems to measure range, and robust under almost all lighting and weather conditions with or without glare and shadows [4].

Notably, autonomous vehicles will implement computer vision algorithms for detecting and classifying objects and obstacles in the surroundings [5], including cars, pedestrians, and road signs. In this context, more robust scene understanding could be achieved if vehicles exchanged their sensor data via Vehicle-To-Everything (V2X) communication to other vehicles and/or road infrastructures. This approach permits to extend the perception range beyond the capabilities of onboard instrumentation, a concept usually referred to as *cooperative perception* [6], [7]. However, transmitting large volumes of data may be challenging for current V2X communication technologies. For example, a raw LiDAR frame is, on average, 1 MB [8]: with a frame rate of 30 fps, it would produce a data rate of around 240 Mbps. For comparison, 3GPP C-V2X and IEEE 802.11p, i.e., the de facto standards for V2X, can offer a nominal data rate of only a few tens of Mbps [9]. One possible method to solve capacity issues is to compress data before transmission, which in turn introduces additional complications [10]. For example, compression may sacrifice accuracy to reduce the file size, with severe implications for the operations that rely on data such as object detection. Moreover, while compressing data from videocameras is relatively straightforward, there is no accepted standard for compression of LiDAR data.

A. Motivations

The design of communication algorithms for autonomous driving requires a rigorous process of validation. To this aim, using a real testbed is impractical due to limitations in scalability, flexibility, and the high cost of hardware components. Theoretical analyses, in turn, often introduce conservative and/or unrealistic assumptions on the system model, and may lead to wrong or misleading conclusions. Simulations, in turn, have the advantage to reduce costs and time consumption for validation, and would facilitate the research process.

To do so, computer simulations need accurate modeling of the different components of the network at all layers. Notably, at the application layer, automotive data is required, which comes with at least three main concerns. First, labeled data are often expensive and time-consuming to generate, or completely unavailable [8]. Second, the dataset shall be available and stored on the simulator machine. For example, SemanticKITTI [11], a popular open-source labeled dataset for autonomous driving research, consists of around 80 GBytes of data, which may consume excessive memory resources. Third, the dataset shall be accessed, saved, and processed in the RAM of the simulator machine, introducing delays that scale with the size of the dataset. In particular, data compression requires point-level processing, which may be hard to perform in real time. For example, geometry-based point cloud (G-PCC) [12], a possible standard for LiDAR compression, can compress only 440k points/s [10] (for comparison, the HDL-64E LiDAR sensor used in SemanticKITTI captures 1.3M points/s). Moreover, data compression involves expensive and energy-consuming hardware (particularly high-end GPUs), which may be unavailable on the simulator machine.

An alternative approach is to simulate the application layer using a statistical model of the automotive data rather than real data. Therefore, the traffic is simulated based on the sole arrival process of packets (especially the packet size and the inter-arrival time) according to some mathematical process, and this approach does not require a dataset to be available and stored on the simulator machine. Our early results indicate that a single simulation in ns-3, a popular full-stack end-to-end network simulator, of 15 s takes on average around 605 s (10 min) to complete using automotive data from SemanticKITTI, vs. only 20 s using the corresponding statistical model.

In the literature, statistical methods have been proposed to model, for example, the propagation of the signal [13], the application (e.g., for web browsing [14] or, more recently, eXtended Reality (XR) traffic [15]) or, in the vehicular domain, automotive radar reflections [16] or multi-sensor data fusions systems [17]. However, to date, there is no universal statistical model for automotive sensor data, particularly for LiDAR point clouds. Ideally, such data could be represented as periodic traffic with a fixed frame rate and a constant frame size proportional to the resolution of the sensor. However, in practice, automotive data is often compressed before transmission to reduce the file size, leading to frames of variable size. Therefore, automotive data should be modeled as a combination of random variables, after proper fitting and validation via statistical methods.

B. Contributions

Based on the above introduction, the contributions of this paper can be summarized as follows.

- We provide a realistic statistical characterization of automotive data, specifically of the size of LiDAR point clouds. To the best of our knowledge, this is the first model for automotive traffic, and is based on the SemanticKITTI dataset. Given the importance of compression in the automotive scenario, we provide seven different models to characterize raw data and six representative compression configurations. Specifically, data is compressed using the state-of-the-art Hybrid Semantic Compression (HSC) algorithm, first proposed in [18], which supports different levels of compression to trade off quality against speed. We claim that the availability of statistical models for automotive data brings several advantages compared to using actual data, including faster simulations and processing at the application layer, and no or limited storage of data.
- We quantify the accuracy of our statistical models. Specifically, we test different distributions, and identify the corresponding fitting parameters. The measure of accuracy is assessed via a custom statistical test based on the Maximum Likelihood Estimation (MLE), Kolmogorov-Smirnoff (KS), and Bootstrap Resampling schemes [19]. Our results show that the size of the uncompressed data can be accurately modeled according to the tLocationScale distribution, while for the compressed data we select the tLocationScale, Nakagami, Logistic or Gamma distributions according to the level of compression. Interestingly, six of the seven models pass the test.
- We further validate the accuracy of our statistical models on representative network metrics via ns-3 simulations. First, we extend the ns-3 code base with new custom methods to generate random variables according to the tLocationScale, Nakagami, and Logistic distributions, which are not natively available in ns-3. Then, we simulate the transmission of automotive data between two vehicles as a function of their distance. At the application layer, we simulate data transmission at the packet level (raw or compressed) using real data from the SemanticKITTI dataset or based on our statistical traffic models, and compare the corresponding network metrics at the Packet Data Convergence Protocol (PDCP) layer. We observe that, even though only six of the seven models passed the test, the statistical approach produces similar, if not the same, results as with real data in terms of end-to-end latency and throughput. This confirms that statistical models can be used to simplify network simulations without compromising the reliability of the results.

The rest of the paper is organized as follows. In Sec. II we present some related works. In Sec. III we briefly describe our system model, specifically the HSC pipeline for data compression. In Sec. IV we formalize our statistical analysis to define accurate models for automotive data, and assess the accuracy of those models. In Sec. V we describe the ns-3 implementation of the random distributions used by the models.

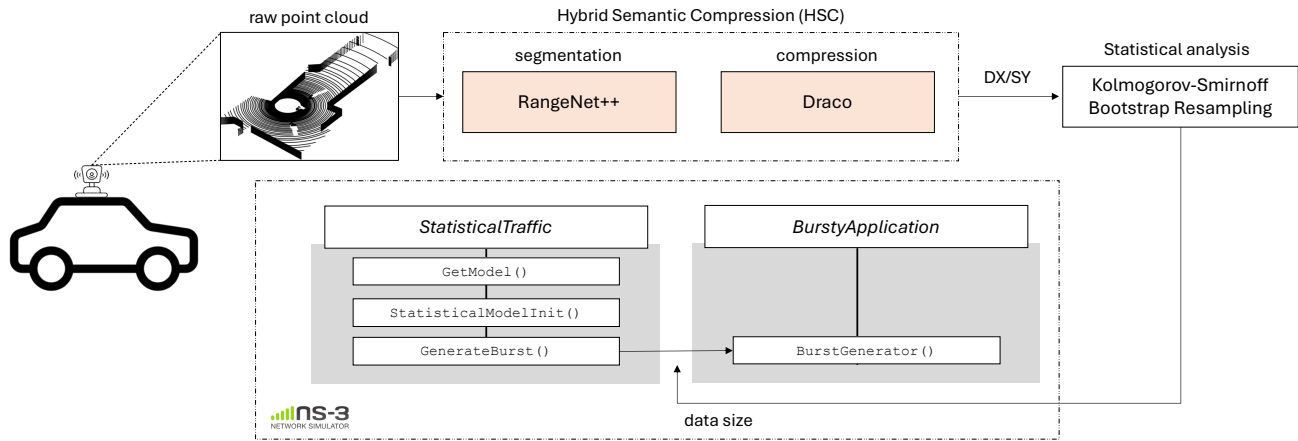


Fig. 1: Overview of the system model. An autonomous vehicle generates 3D LiDAR point clouds, which may be compressed via Hybrid Semantic Compression (HSC) to reduce the file size. Statistical analysis via Kolmogorov-Smirnoff (KS) and Bootstrap Resampling methods is performed to identify statistical models for the size of 3D LiDAR point clouds. The accuracy of the models is assessed via statistical tests, and based on their impact on network metrics, measured via ns-3 simulations.

In Sec. VI we present simulation results to evaluate the impact of the models on the network under several metrics. Finally, conclusions and suggestions for future work are discussed in Sec. VII.

II. RELATED WORK

V2X communication, both among vehicles and/or with the network, is a key enabler of the autonomous driving revolution. However, it comes with several challenges, due to the large size of the data [20], the highly dynamic and heterogeneous road environment, as well as the stringent network requirements of autonomous driving [21]. In this sense, a complete characterization of the traffic generated by autonomous vehicles is essential to design the appropriate V2X communication technologies and protocols. Furthermore, as network functions become increasingly virtualized, traffic modeling is critical for proper network dimensioning [22]. Additionally, (generative) traffic models play a crucial role in network simulations, significantly reducing both the cost and time required for implementing and testing new solutions and architectures [23]. For these reasons, modeling the network traffic has been a central research topic for the last decades.

Authors in [24] presented an extensive list of traffic models for 5th Generation (5G) applications, though with limited references to the autonomous driving scenario. Several works modeled the data stream for Internet of Things (IoT) applications. Specifically, the authors in [25] modeled the aggregated Machine-to-Machine (M2M) traffic and the corresponding message delivery delay in a 5G network, while papers [26] and [27] focused on a single traffic source, deriving stochastic models based on Markov Chains. In addition, the survey in [28] reported an overview of traffic models for Peer-to-Peer (P2P) communication in IoT blockchain networks. The traffic generated by video streaming has also been extensively investigated [29]. For example, Kalbkhani *et al.* [30] proposed to use non-linear autoregressive models to predict the future frame size in video traffic. Besides classic video applications, the research community is working on the characterization

of interactive video traffic for XR applications, e.g., in [31], [32]. In addition to the more classical models based on state machine and autoregression techniques [26], [27], [33], more recently Machine and Deep Learning techniques were employed to model complex traffic patterns. For instance, Nie *et al.* [34] combined a deep-belief network with a compressed-sensing approach to predict the fast- and slow-varying traffic components in a wireless mesh network. Other works such as [35], [36] introduced long short-term memory (LSTM) models to capture and forecast network traffic statistics.

For the specific case of autonomous driving, only a few studies have specifically addressed the characterization of the network traffic. For example, Choi *et al.* [20] characterized the data rates of different automotive sensors, using information obtained from the datasheets of commercial products and conversations with industrial partners; for LiDAR (videocamera) sensors, the resulting data rate was measured between 10 and 100 (100 and 700) Mbps depending of the resolution. Grigoreva *et al.* [33] further introduced a machine-type communication traffic model tailored to automotive applications, incorporating spatial and temporal correlations. Wang *et al.* [37] measured the mean frame size, frame rate, and delay of sensor data based on an experimental demo system, providing additional empirical insights. Similarly, the data rate of the commercial Velodyne HDL-64E LiDAR sensor was characterized in [38]. However, these models have been obtained for specific types of sensors, and only model the data rate of the sensors. A comprehensive, closed-form, and statistical characterization of automotive data is still an open challenge, which motivates the research presented in this paper.

III. SYSTEM MODEL

In this section we present our system model, also illustrated in Fig. 1, specifically the automotive data (Sec. III-A), the HSC compression pipeline (Sec. III-B), and the selection process to identify the types of data to be analyzed in this paper (Sec. III-C),

A. Automotive Data

Autonomous vehicles rely on a combination of multiple sensors to perceive their surroundings. In addition to video-cameras, LiDAR sensors are often used, given their ability to provide accurate distance measurements in different lighting and weather conditions. Therefore, in this paper we propose a statistical characterization of the size of automotive data focusing on LiDAR sensors, and based on SemanticKITTI [11], a large-scale, high-resolution dataset designed for semantic segmentation tasks in autonomous driving research. It extends the popular KITTI Vision Benchmark Suite by providing dense, point-wise annotations for LiDAR data collected using a Velodyne HDL-64E sensor. The dataset consists of 22 sequences, for a total of 43 552 LiDAR scans, captured in diverse environments such as urban streets, rural areas, and highways. Each point in the 3D point cloud is annotated based on 28 semantic classes, including road, building, vegetation, and dynamic objects like cars, pedestrians, and cyclists.

B. Hybrid Semantic Compression (HSC)

Data transmission is challenging, given the large size of LiDAR point clouds. For SemanticKITTI, each raw LiDAR acquisition generates a point cloud of around 120 000 points, with an average file size of around 3 200 KB. Therefore, data should be processed, e.g., compressed, before transmission, to reduce the file size and so the link overload.

In [18], we proposed a compression pipeline for LiDAR data called HSC, which exploits the semantic understanding of the 3D scene to reduce the size of point clouds. The HSC pipeline consists of two modules: a Deep Learning semantic module (based on RangeNet++ [39]) to select safety-critical points, and a compression module (based on Google Draco [40]) to compress the resulting point cloud at fast speed. Specifically, we consider three Semantic Levels (SLs): SL = 0, representing raw data before compression; SL = 1, where we remove points from the point cloud relative to the road and the background; and SL = 2, where points from buildings, vegetation, and traffic signs are also removed. For compression, Draco relies on two parameters: the Quantization Parameter (QP) $\in \{1, \dots, 14\} \cup \{0\}$, i.e., the number of bits used for quantizing input values, with QP = 0 indicating no quantization; and the Compression Level (CL) $\in \{0, \dots, 10\}$, which trades off compression accuracy over efficiency (measured in terms of the encoding and decoding time). More precisely, higher values of CL achieve better compression, at the cost of a slower encoding or decoding.

C. Data Selection Process

Overall, HSC results in a rich set of (almost 500) possible compression configurations, offering a fine-grained control over the compression performance. However, for simplicity, in this work we decided to consider only a selection of seven representative compression configurations. Specifically, we inspected the rendered point clouds after Draco compression, and grouped similar configurations based on (i) the impact of compression on the quality of data, and (ii) the average encoding and decoding

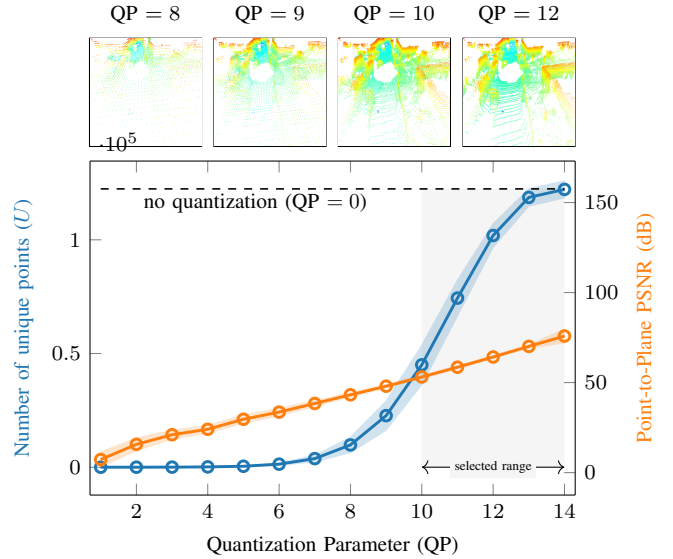


Fig. 2: Number of unique points U and p2p-PSNR after compression vs. QP. Above, random point clouds from SemanticKITTI after compression for QP $\in \{8, 9, 10, 12\}$.

time. Assuming that, for lossy compression, the main source of distortion is quantization, we investigate the effect of QP on the compressed point clouds, and study the encoding and decoding time as a function of CL.

1) *Compression quality analysis:* The semantic understanding of data, e.g., detection and classification of objects in the environment, is a key component for the development of reliable autonomous vehicles [41], [42], [43], [44], [45]. However, the semantic performance may rapidly deteriorate due to lossy compression of the input [46], [47], [48].

Thus, we analyze the impact of HSC Draco compression on the quality of LiDAR point clouds. Specifically, we set CL = 7, and vary QP from 0 to 14 as per Draco’s specifications. Then, we compute:

- The number U of unique points in the compressed point cloud: Draco preserves the number of points between input and output but, as a result of the compression process, it condenses multiple points into a single one, reducing the number of unique points in the compressed point cloud.
- The Point-to-Plane PSNR (p2p-PSNR) [49] to quantify the geometric distortion of point cloud compression based on the Peak Signal to Noise Ratio (PSNR).

Both metrics are computed and averaged over a sample of 550 LiDAR point clouds, uniformly selected from the SemanticKITTI dataset. In Fig. 2 we plot U and p2p-PSNR as a function of QP, and also report random point cloud samples from SemanticKITTI for QP $\in \{8, 9, 10, 12\}$ for a qualitative evaluation. We observe that, for QP ≤ 10 , compression is overly aggressive as the visual quality of the point clouds is severely degraded. Furthermore, at QP = 10, we empirically notice a change in the slope of the p2p-PSNR curve from approximately 5 dB/QP to 6.25 dB/QP, as well as a decrease of the number of unique post-compression points by approximately 70%. Hence, based on these observations, we selected QP values in the range $\{10, 11, 12, 13, 14, \} \cup \{0\}$. Notice that this analysis is consistent with the algorithm

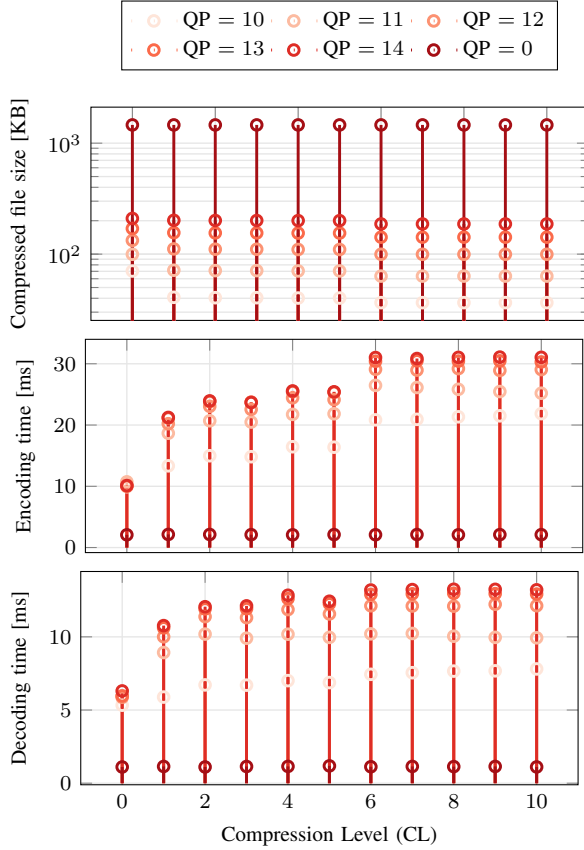


Fig. 3: Average file size and encoding/decoding time vs. $CL \in \{0, 1, \dots, 10\}$, and for $QP \in \{0, 10, 11, 12, 13, 14\}$.

description in the Draco repository,¹ where it is stated that “most projects can set quantization values of about 11 without any noticeable difference in quality”.

2) *Compression time analysis:* Based on the values of QP previously selected, we now calculate the file size, encoding time, and decoding time for compression vs. $CL \in \{0, 1, \dots, 10\}$.² In Fig. 3 we observe that, for a fixed value of QP, the file size does not significantly change as a function of CL. Conversely, we see that the encoding and decoding times increase as CL increases, especially for $CL \geq 5$, with marginal effects on the file size. Moreover, the curves almost overlap for $QP \in \{12, 13, 14\}$. For this reason, we choose the corner case $QP = 14$ as a cluster representative, and fix $CL = 5$ as it represents a sweet spot between file size and encoding/decoding time.

3) *Final selection:* In summary, we select a subset of Draco configurations that are deemed qualitatively acceptable and most relevant for LiDAR automotive data, specifically $QP \in \{10, 11, 14\}$ and $CL = 5$. Combined with the three SLs of HSC, we define 9 models, identified as **DX/SY**, where X is the QP, and Y is for the $SL \in \{0, 1, 2\}$. We use the value X

¹Draco code repository: <https://github.com/google/draco>

²Note that the parameter combination $\{QP=0, CL=0\}$ does not disable Draco, thus it does not correspond to raw data. In fact, while the raw data file from SemanticKITTI has the extension .ply, the output file after Draco is applied has extension .drc, regardless of the compression mode, which is a more efficient data format representation. This also explains why the encoding and decoding times are not zero in this case.

$= 0$ to represent the configuration where Draco is disabled. For example, D0/S0 identifies raw data, and D0/S1 represents raw data with $SL = 1$. Finally, to further reduce the number of combinations to analyze, we neglect $QP = 10$, and consider only $SL = 0$ for $QP = 11$ (D11/S0), which represents a pure Draco compression with no HSC semantic module. In this way, the cardinality of the model space is effectively reduced to seven combinations: D0/S0, D0/S1, D0/S2, D11/S0, D14/S0, D14/S1, and D14/S2.

In the next section, we will provide statistically representative traffic models to characterize the size of LiDAR data based on the seven HSC configurations selected above.

IV. STATISTICAL MODELS FOR AUTOMOTIVE DATA

Assuming a constant generation interval for LiDAR data (typically 10 or 30 fps), the size of the point clouds to be transmitted is the most relevant element to be considered when characterizing the source traffic. Thus, we consider the SemanticKITTI dataset [11], and evaluate the Cumulative Distribution Functions (CDFs) of the size of LiDAR point clouds for each of the compression configurations defined in Sec. III-C. In Sec. IV-A we describe our statistical method, while validation results are reported in Sec. IV-B.

Notation: We denote vectors as bold, lower case letters.

A. Statistical Method

For each compression configuration, we consider a diverse set \mathbb{P} of theoretical CDF families as potential candidates for the unknown target CDF F that represents the size of such data. A hypothetical CDF F_i , $i \in \{1, 2, \dots, |\mathbb{P}|\}$, is tested against the empirical CDF (eCDF) $\hat{F}^{(N)}$ derived from a random sample of N observations from F . This is a well-known procedure called hypothesis testing. Specifically, in this work we perform a KS test [50] to compare F_i and $\hat{F}^{(N)}$ based on the KS statistic $D^{(N)}$, which quantifies the “distance” between the hypothetical distribution and the distribution of the observed data, i.e.,

$$D^{(N)}(i) = \max_x |\hat{F}^{(N)}(x) - F_i(x)|. \quad (1)$$

In general, for continuous CDFs and assuming that the two samples $\hat{F}^{(N)}(x)$ and $F_i(x)$ come from the same distribution (null hypothesis), $\hat{F}^{(N)} \rightarrow F_i$ as $N \rightarrow \infty$ (strong law of large numbers), thereby $D^{(N)}(i)$ converges to zero almost surely. Moreover, under the same hypothesis, the limiting distribution of $\sqrt{N}D^{(N)}(i)$ converges to a Kolmogorov distribution, independent of F_i . As a result, under the null hypothesis and for N sufficiently large, Eq. (1) has a known distribution, and well-known critical values. Notice that the interpretation of the KS statistic centers around the p-value and a predefined significance level α : if the p-value is less than α , the test concludes that the null hypothesis is unlikely to be true, and that it shall be rejected, i.e., the test is not passed for F_i . For ease of notation, we will write \hat{F} and D instead of $\hat{F}^{(N)}$ and $D^{(N)}$, respectively, where the dependence on N is implicit, unless stated otherwise.

We denote the set of 3D LiDAR point clouds in the SemanticKITTI dataset as

$$\mathcal{D} = \{\mathbf{p}_j : \mathbf{p}_j \in \mathbb{R}^{3 \times n_j}, j = 1, \dots, N\}, \quad (2)$$

TABLE I: P-values $\pi_{i,m}^*$ computed according to Eq. (8), where $i \in \mathbb{P}$ represents the row index, while m is the column index and identifies the HSC compression configuration under test. For each configuration, we represent in bold the p-values that pass the test, i.e., $\pi_{i,m}^* \in \mathcal{I}_m$, and highlight in gray the entries selected as best fits, that is i_m^* .

\mathbb{P}	D0/S0	D0/S1	D0/S2	D11/S0	D14/S0	D14/S1	D14/S2
BirnbaumSaunders	0	0.0	0.061	0.013	0.0	0.0	0.0
ExtremeValue	0	0.0	0.0	0.0	0.0	0.003	0.0
Gamma	0	0.0	0.375	0.114	0.0	0.0	0.012
GeneralizedExtremeValue	0	0.003	0.039	0.006	0.0	0.0	0.0
HalfNormal	0	0.0	0.003	0.0	0.0	0.0	0.0
InverseGaussian	0	0.0	0.002	0.018	0.0	0.0	0.0
Logistic	0	0.009	0.0	0.0	0.036	0.024	0.0
Loglogistic	0	0.0	0.018	0.037	0.01	0.0	0.0
Lognormal	0	0.0	0.065	0.02	0.0	0.0	0.0
Nakagami	0	0.001	0.0	0.128	0.0	0.0	0.004
Normal	0	0.109	0.0	0.012	0.0	0.0	0.0
Poisson	0	0.0	0.0	0.0	0.007	0.0	0.0
Rayleigh	0	0.0	0.0	0.0	0.0	0.0	0.0
tLocationScale	0	0.029	0.0	0.014	0.026	0.026	0.0
Weibull	0	0.044	0.15	0.0	0.003	0.0	0.01

where n_j is the number of points in the point cloud $\mathbf{p}_j \in \mathcal{D}$. We represent each HSC compression configuration (denoted by DX/SY) by a function $m : \mathcal{D} \rightarrow \hat{\mathcal{D}}$ that receives as input a point cloud $\mathbf{p} \in \mathcal{D}$, and gives as output its compressed version $\hat{\mathbf{p}} \in \hat{\mathcal{D}}$. Then, we denote as B_m the set of sizes of the point clouds in $\hat{\mathcal{D}}$, compressed using configuration m , i.e.,

$$B_m(\hat{\mathcal{D}}) = \{b_j \in \mathbb{R} : b_j = g(\hat{\mathbf{p}}_j), \quad (3)$$

$$\hat{\mathbf{p}}_j = m(\mathbf{p}_j) \in \hat{\mathcal{D}}, \quad j = 1, \dots, N\}, \quad (4)$$

where $g(\mathbf{p})$ corresponds to the number of bits used to encode \mathbf{p} , i.e., the size of \mathbf{p} . The goal of our analysis is to find, for each compression configuration m , the class of functions $\mathcal{P}_i = \{F_i(\cdot; \boldsymbol{\theta}) : \boldsymbol{\theta} \in \Theta_i\} \in \mathbb{P}$, in the presence of unknown parameters $\boldsymbol{\theta} \in \Theta_i$, and the corresponding CDF $F_i(\cdot; \boldsymbol{\theta}_i)$, $i \in \{1, 2, \dots, |\mathbb{P}|\}$ (our hypothesis, where $\boldsymbol{\theta}_i$ is a specific realization of $\boldsymbol{\theta}$), that best fit $B_m(\hat{\mathcal{D}})$ (sample of observation) according to some evaluation metric $h_m : \mathcal{P}_i \rightarrow \mathbb{R}$. In other words, our goal is to perform a goodness-of-fit test for each class \mathcal{P}_i . For example, if \mathcal{P}_i is the family of Normal distributions, the unknown parameters are $\boldsymbol{\theta} = (\mu, \sigma^2) \in \mathbb{R}^2$.

We design the statistical test by first estimating some parameters $\hat{\boldsymbol{\theta}}_i$ for each class \mathcal{P}_i , so as to identify a representative CDF $F_i(\cdot; \hat{\boldsymbol{\theta}}_i)$. Then, we perform a KS goodness-of-fitting test for this representative distribution. However, estimating $\hat{\boldsymbol{\theta}}_i$ from the observed data can alter the asymptotic distribution of the test statistic in Eq. (1), rendering it dependent on these parameters. Consequently, even under the null hypothesis, the distribution may deviate from the Kolmogorov distribution, and require a recalibration of the critical values [51]. To address this issue, we adopt a parametric Bootstrap Resampling scheme as proposed in [51], [52], and described in the following steps.

1) *Parameter Estimation*: For each class $\mathcal{P}_i \in \mathbb{P}$, $i \in \{1, 2, \dots, |\mathbb{P}|\}$, we compute the Maximum Likelihood Estimation (MLE) from the observed data $B_m(\hat{\mathcal{D}})$ to estimate $\hat{\boldsymbol{\theta}}_i$. Then, we select CDF $F_i(\cdot; \hat{\boldsymbol{\theta}}_i) \in \mathcal{P}_i$ as a representative distribution for class \mathcal{P}_i , thus as the model being tested.

2) *Target KS Statistic*: We define the composite null hypothesis of the statistical test as

$$H_0^i : \text{draw samples from } F_i(\cdot; \hat{\boldsymbol{\theta}}_i), \quad (5)$$

TABLE II: Parameters for the selected statistical models based on Table I.

m	Distribution \mathbb{P}	Parameters	Values
D0/S0	tLocationScale	μ, σ, ν	3172.74, 64.41, 1.49
D0/S1	Normal	μ, σ	1458.7, 455.36
D0/S2	Gamma	a, b	1.87, 131.97
D11/S0	Nakagami	μ, ω	9.31, 4914.06
D14/S0	Logistic	μ, σ	197.54, 8.96
D14/S1	tLocationScale	μ, σ, ν	98.11, 16.83, 4.08
D14/S2	Gamma	a, b	2.81, 6.06

and compute the KS statistic as

$$D(i) = \max_{x \in B_m(\hat{\mathcal{D}})} |\tilde{F}(x) - F_i(x; \hat{\boldsymbol{\theta}}_i)|, \quad (6)$$

where \tilde{F} is the empirical CDF of the observed set $B_m(\hat{\mathcal{D}})$. Notice that the hypothetical CDF $F_i(\cdot; \hat{\boldsymbol{\theta}}_i)$ depends on $B_m(\hat{\mathcal{D}})$, and $D(i)$ is no longer distribution-free. Therefore, a Bootstrap Resampling scheme is necessary.

3) *Parametric Bootstrap Resampling scheme*: We define L independent Bootstrap resamples $\{B_{m,l}^*(\hat{\mathcal{D}})\}_{l=1}^L$ from the estimated population $F_i(\cdot; \hat{\boldsymbol{\theta}}_i)$ and, for each $B_{m,l}^*(\hat{\mathcal{D}})$, we compute the MLE to estimate $\hat{\boldsymbol{\theta}}_{i,l}^*$. Our goal is to obtain L KS statistics, and compare them with the target statistics in Eq. (6). We denote as $\tilde{F}_l(x)$ the empirical CDF of $B_{m,l}^*(\hat{\mathcal{D}})$. Then, the KS statistic computed on the l -th Bootstrap resample is

$$D_l(i) = \max_{x \in B_{m,l}^*(\hat{\mathcal{D}})} |\tilde{F}_l(x) - F_i(x; \hat{\boldsymbol{\theta}}_{i,l}^*)|. \quad (7)$$

Since $\sqrt{N}(\tilde{F}(x) - F_i(x; \hat{\boldsymbol{\theta}}_i))$ and $\sqrt{N}(\tilde{F}_l(x) - F_i(x; \hat{\boldsymbol{\theta}}_{i,l}^*))$ converge to the same Gaussian process, $\sqrt{N}D(i)$ and $\sqrt{N}D_l(i)$ have the same limiting distribution [52]. Therefore, the critical values relative to Eq. (6) can be obtained computing the $(1-\alpha)$ -percentile of $\{\sqrt{N}D_l(i)\}_{l=1}^L$, where α is the significance level. Equivalently, we can compute the Bootstrap p-value $\pi_{i,m}^*$ as

$$\pi_{i,m}^* = \frac{1}{L} \sum_{l=1}^L \mathbb{1}_{\{D_l(i) > D(i)\}} \quad (8)$$

$$= 1 - \tilde{F}_{D^*(i)}(D(i)) \approx \text{Prob}(D^*(i) > D(i)), \quad (9)$$

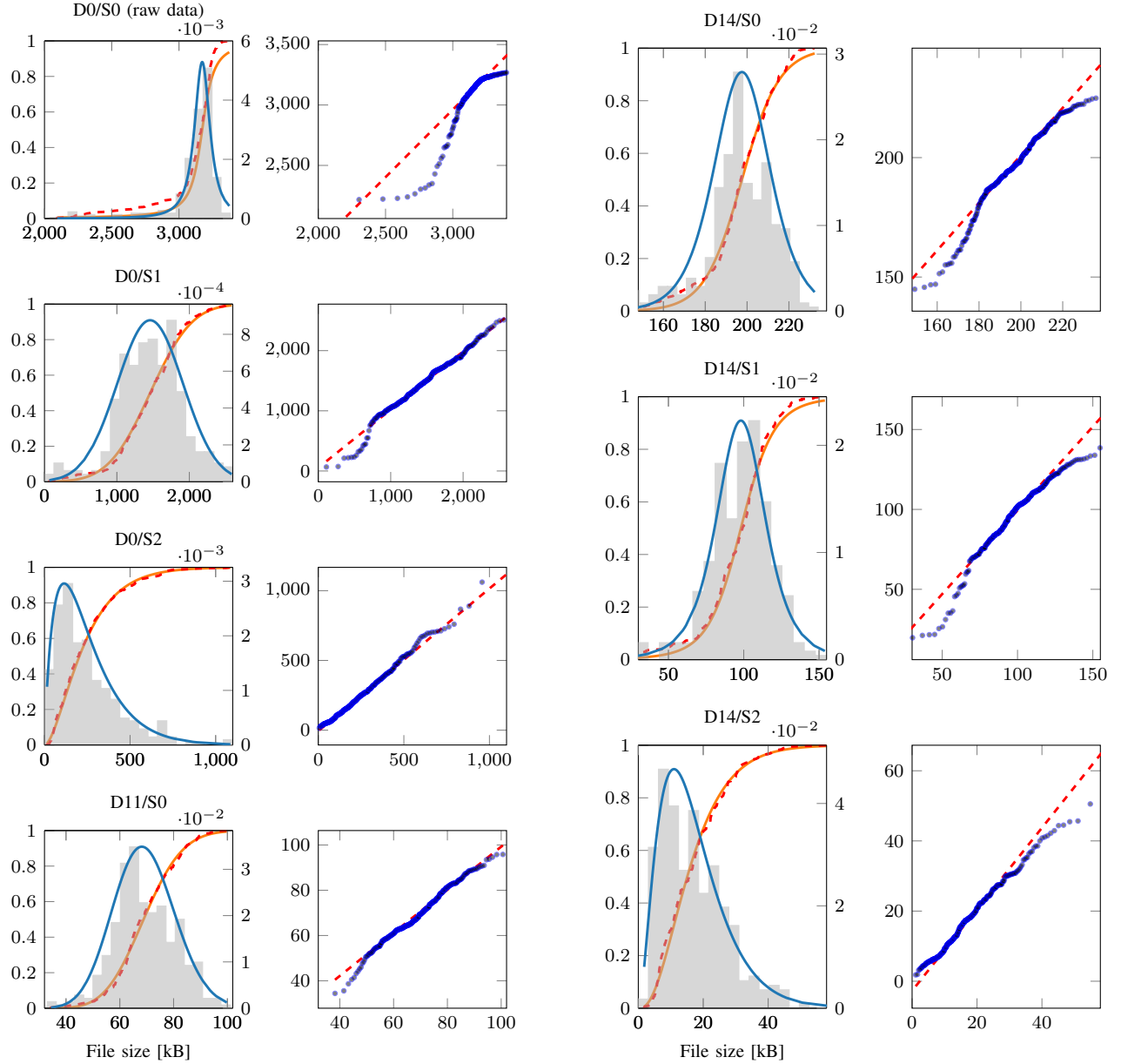


Fig. 4: Fitting plots: data histogram (light grey), empirical CDF (dashed red), fitted PDF (light blue), fitted CDF (orange), and QQ-plots (right).

where $\tilde{F}_{D^*(i)}(D(i))$ is the empirical CDF of $\{D_l(i)\}_{l=1}^L$. Therefore, H_0^i can be rejected at significance level α if $\pi_{i,m}^* < \alpha$, i.e., $\text{Prob}(D^*(i) \leq D(i)) > 1 - \alpha$.

4) *Model Selection*: The KS statistical test with the Bootstrap Resampling scheme described above provides, for each configuration m , $|\mathbb{P}|$ statistical test outcomes, one for each distribution family. We define the set of indices of distribution families for which the null hypothesis cannot be rejected as \mathcal{J}_m . Then, we select as best fit the CDF family $\mathcal{P}_{i_m^*}$ and $F_{i_m^*}(\cdot; \hat{\theta}_{i_m^*})$, $\forall i \in \mathcal{J}_m$, such that $i_m^* = \arg \max_{i \in \mathcal{J}_m} \pi_{i,m}^*$. If $\mathcal{J}_m = \emptyset$, we select as best fit the model that minimizes the Normalized Root Mean Squared Error (NRMSE), computed as

$$\text{NRMSE} = \sqrt{\frac{\sum_{k=1}^N (\tilde{F}(x_k) - F_i(x_k; \hat{\theta}_i))^2}{\sum_{k=1}^N (\tilde{F}(x_k) - \bar{F}_i(\hat{\theta}_i))^2}}, \quad (10)$$

where $\bar{F}_i(\hat{\theta}_i) = \frac{1}{N} \sum_{k=1}^N F_i(x_k; \hat{\theta}_i)$.

B. Statistical Results

In this section we present and discuss the results obtained from the statistical method in Sec. IV-A. Table I shows the Bootstrap p-values $\pi_{i,m}^*$ computed according to Eq. (8) for each compression configuration m , and considering several CDF families. We set $\alpha = 0.01$ and $L = 1000$. We represent in bold the p-values that pass the test, i.e., $\pi_{i,m}^* \in \mathcal{I}_m$, and highlight in grey the entries selected as best fits, that is i_m^* . We see that the size of LiDAR point clouds can be represented as tLocationScale, Nakagami, Normal and Logistic distributions, depending on the compression configuration. Notice that D0/S0 is the only model that does not pass the test ($\mathcal{I}_m = \emptyset$). In this case, we choose as best fit the distribution with the minimum NRMSE, i.e., tLocationScale, for which $\text{NRMSE} = 7.4 \cdot 10^{-3}$.

Finally, in Table II we report the parameters $\hat{\theta}_{i^*}$ for the best fitting models, that will be used in the ns-3 implementation (Sec. V) and the end-to-end performance evaluation (Sec. VI).

Moreover, we complement this numerical analysis with fitting plots. Specifically, for each model, Fig. 4 illustrates the empirical CDF \hat{F} and Probability Density Function (PDF) of the observed data, as well as the validated theoretical CDF $F_{i^*}(\cdot; \hat{\theta}_{i^*})$, together with the QQ-plot (Quantile-Quantile plot). The latter serves as a graphical diagnostic method to visually compare two distributions. It plots on the x-axis the quantile function of one distribution and on the y-axis the quantile function of the other distribution. Therefore, if two distributions are identical, the QQ-plot will lie along the bisector of the first quadrant. We see that the PDF and CDF of all the models generally fit the empirical data, confirming the accuracy of our statistical results. The QQ-plots also show good accuracy, with only minor deviations in the tails, which decrease as the semantic level (S0, S1, S2) increases. This is probably due to the fact that, as fewer points remain in the point cloud, the structure of the resulting data is less complex, which facilitates a better fit to a statistical distribution. The only exception is for the D0/S0 model, where the QQ-plot reveals a heavy left tail, which highlights some discrepancy between the statistical and empirical distributions. This is consistent with the fact that D0/S0 is the only model that fails the test.

V. NS-3 IMPLEMENTATION OF STATISTICAL MODELS

In this paper, we measure the accuracy of the proposed statistical models for the size of automotive data based on their impact on network metrics. To do so, we use ns-3 as a default system-level simulator [53]. Notably, ns-3 has gained great popularity within the network simulation community. It consists of a large set of predefined, scalable, ready-to-use, open-access modules to simulate different parts of the (wireless) network. It also comes with modules to simulate V2X networks based on the most recent 3rd Generation Partnership Project (3GPP) specification for NR V2X [54], mobility traces using SUMO [55], and a pipeline to simulate and test machine learning algorithms within the Radio Access Network (RAN) [56]. As such, it stands out as one of the most complete 5G-oriented tools to perform accurate simulations in the context of vehicular networks. In Sec. V-A we describe the ns-3 application model, and in Sec. V-B we focus on the implementation of the statistical models in ns-3, which we validate in Sec. V-C.

A. Application Model

The statistical models have been implemented at the application layer of ns-3 in the new *StatisticalTraffic* module, which we made publicly available.³ Given the nature of point clouds, it is built on top of the *BurstyApplication* [57], originally designed to model XR traffic. Specifically, it serves as a bursty traffic generator that produces bursts of network packets based on two input parameters: the size of LiDAR point clouds, modeled

based on the statistical distributions presented in Sec. IV-B, and a predefined inter-arrival time.

Notably, the proposed *StatisticalTraffic* module simulates the packet generation process for the seven different HSC compression configurations presented in Sec. III-C. First, the application selects the point cloud size distribution through the `GetModel` routine. Then, the `StatisticModelInit` routine initializes the distribution parameters according to Table II. Finally, the `BurstSize` and `FramePeriod` are generated based on the corresponding statistical models, and passed to the *BurstyApplication* through the `BurstGenerator` interface. Fig. 1 depicts a block diagram of the ns-3 module.

The remaining components of the 5G NR V2X protocol stack are emulated using the *mmWave* module [58]. This module features a customized Physical (PHY) layer that accommodates 5G New Radio (NR) frame formats and numerologies, as well as a Medium Access Control (MAC) layer supporting ad hoc beamforming and scheduling strategies. The PDCP layer leverages the ns-3 *Lena* module for Long Term Evolution (LTE) networks [59], providing network functions such as packet segmentation, retransmissions, and reassembly. Furthermore, this module facilitates non-standalone deployments, handovers, and mobility management through dual connections, along with Carrier Aggregation (CA) at the MAC layer.

B. Implementation Details of Statistical Distributions

The implementation of *StatisticalTraffic* requires the integration of statistical distributions directly within the ns-3 framework. Although ns-3 offers built-in support for a wide range of random variables, it does not implement the `tLocationScale`, Logistic and Nakagami distributions, which are essential for the proposed traffic models. For `tLocationScale` and Logistic, we use the Inverse Cumulative Distribution Function (Inverse CDF) sampling method, a well-known statistical technique used to generate random samples from a probability distribution with a known CDF. It involves mapping uniformly distributed random numbers (typically between 0 and 1) to specific quantiles of the desired distribution using the inverse of the CDF. For Nakagami, we exploit the fact that it can be expressed as a function of a Gamma distribution. Below, we provide a mathematical description for these distributions.

1) *tLocationScale*: The direct implementation of the Inverse CDF for `tLocationScale` is known to be NP-hard. Consequently, various alternative approaches have been proposed [60]. In our implementation, we utilize the central power series method. Thus, we represent the Inverse CDF of `tLocationScale` as

$$F_{\text{tloc}}^{-1}(u; \mu, \sigma, \nu) = \left(\nu + \sum_{i=1}^{\infty} c(i, \nu) V(\nu, u)^{2i+1} \right) \sigma + \mu, \quad (11)$$

where μ , σ and ν are the location, scale and shape parameters in Table II, and $V(\nu, u)$ is determined according to

$$V(\nu, u) = \sqrt{\nu\pi} \left(u - \frac{1}{2} \right) \frac{\Gamma(\nu/2)}{\Gamma((\nu+1)/2)}, \quad (12)$$

where $c(i, \nu)$ represents the coefficients of the power series reported in [60, Sec. 5].

³The source code of the ns-3 *StatisticalTraffic* module: <https://github.com/signalabdei/kitti-statistical-dataset>.

TABLE III: P-values of the implemented distributions in ns-3. We represent in bold the p-values that pass the test.

\mathbb{P}	p-value
tLocationScale (\sim Inverse CDF sampling method)	0.296
Logistic (\sim Inverse CDF sampling method)	0.880
Nakagami (\sim Gamma CDF)	0.702

TABLE IV: Network simulation parameters.

Parameter	Value
Carrier frequency	28 GHz
Bandwidth	200 MHz
Transmit Power	30 dBm
Channel Model	3GPP TR 38.901 (UMi-Street Canyon) [62]
LiDAR Inter Burst Interval	100 ms
Buffer Size	12 MB
Data direction	Uplink

2) *Logistic*: In order to implement Inverse CDF of a Logistic distribution, we follow the process outlined in [61]. Specifically, the Inverse CDF can be expressed as a function of the location and scale parameters μ and σ in Table II as

$$F_{\log}^{-1}(u; \mu, \sigma) = \mu - \sigma \ln \frac{1-u}{u}. \quad (13)$$

Thus, a sample from a Logistic distribution can be generated by drawing a number according to a uniform distribution $u \sim \mathcal{U}(0, 1)$, and mapping it through Eq. (13).

3) *Nakagami*: The CDF of a Nakagami distribution can be explicitly derived from the Gamma distribution F_{Γ} , which is natively implemented in ns-3. Therefore, we use a random number generator for F_{Γ} , and adapt it according to

$$F_{\text{nak}}(x; \mu, \omega) = \sqrt{F_{\Gamma}\left(x; \mu, \frac{\omega}{\mu}\right)}, \quad (14)$$

where μ and ω represent the shape and spread parameters in Table II, respectively.

C. Implementation Validation

We test our implemented ns-3 distributions against the corresponding built-in distributions in the Python module *Scipy*. Specifically, we perform a KS test at a significance level $\alpha = 0.05$ to assess whether a sample drawn from our ns-3 implementation of the tLocationScale, Logistic, and Nakagami distributions matches the one from *Scipy*. The p-values of the tests are reported in Table III. We can see that, in all the models, the null hypothesis cannot be rejected since the p-values are far greater than the significance level, which validates the accuracy of our ns-3 implementations.

VI. NETWORK PERFORMANCE EVALUATION OF STATISTICAL MODELS

While in Sec. IV-B we validated the proposed traffic models via statistical tests, we now evaluate their accuracy based on the effect on some network metrics such as latency and throughput via ns-3 simulations. The goal is to verify that statistical models can effectively represent an alternative to real data, provided that the network performance remains consistent in terms of both values and overall trends. In Sec. VI-A we describe our simulation setup and parameters, while in Sec. VI-B we present our numerical results.

TABLE V: Mean PRR vs. d .

d [m]	15-45	75	105	135	165	195	225	255	300
PRR	100.0	82.8	74.5	65.4	48.3	41.2	34.3	16.8	14.0

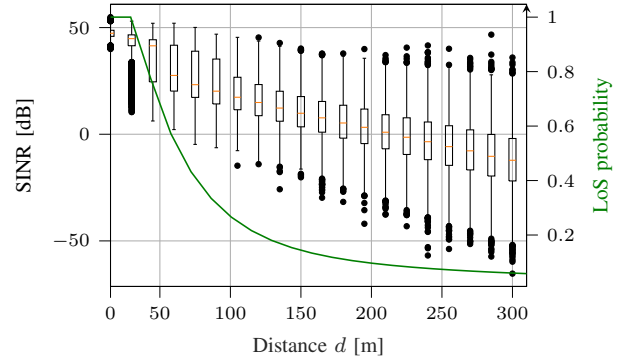


Fig. 5: SINR and LoS probability (based on the model in [62]) vs. d .

A. Simulation Setup

We consider a simple yet realistic urban scenario, where a vehicle transmits LiDAR data to a Next Generation Node Base (gNB) through a millimeter wave (mmWave) link at 28 GHz. The two nodes have the same height, and the distance d between them is increased from 15 to 300 m as the vehicle moves away from the gNB.

We run ns-3 simulations using the parameters reported in Table IV. The channel is simulated according to the 3GPP TR 38.901 UMi-Street Canyon model [62]. Both the gNB and the vehicle are equipped with an 8×8 Uniform Planar Array (UPA), and the beamforming vectors are computed based on the Singular Value Decomposition (SVD) of the channel matrix.

At the application layer, LiDAR bursts are generated every 100 ms. The data is compressed using HSC at the PDCP layer according to the 7 representative configurations introduced in Sec. III-C3: D0/S0, D0/S1, D0/S2, D11/S0, D14/S0, D14/S1, D14/S2. We measure the following End-to-End (E2E) metrics at the PDCP layer: (i) E2E throughput, measured as the ratio between the number of bytes received over the entire simulation and the total simulation time; and (ii) E2E latency, measured as the difference between the time at which each packet is generated at the application layer and when it is successfully received (which accounts for the transmission, compression, queuing, and decompression times).

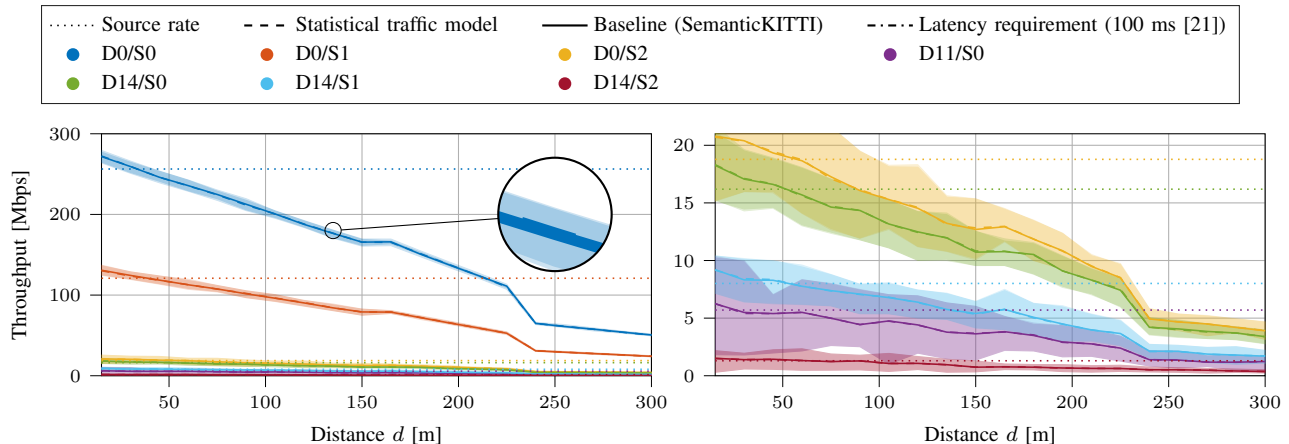
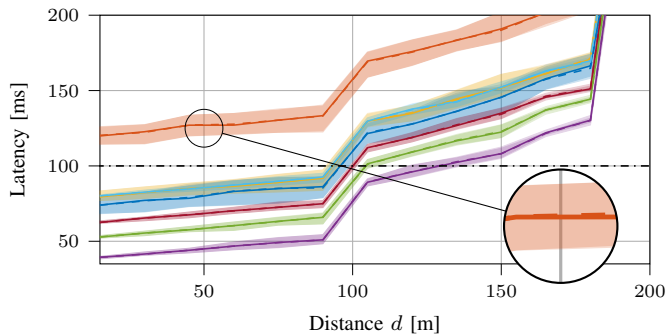
B. Simulation Results

In this section, we compare the network performance obtained using real data from the SemanticKITTI dataset [11], vs. considering our statistical traffic models. Hence, the data size of the point clouds, whether extracted directly from SemanticKITTI or sampled from random distributions, is used in the *BurstyApplication* or *StatisticalTraffic* modules in ns-3, respectively, which in turn generates a stream of packets according to the procedure described in Sec. V.

1) *SINR and PRR*: In Fig. 5 we plot the average Signal to Interference plus Noise Ratio (SINR) as a function of d . We observe that, as expected, at short distances the SINR is

TABLE VI: (Measured) encoding/decoding/inference time, and (simulated) source rate and throughput for different HSC compression configurations.

Parameter	D0/S0	D0/S1	D0/S2	D11/S0	D14/S0	D14/S1	D14/S2
Avg. size [MB]	3.204	1.511	0.235	0.071	0.202	0.100	0.016
Encoding time [ms]	0	0	0	23.3	28.2	12.97	1.95
Decoding time [ms]	0	0	0	10.48	13.57	5.81	0.72
RangeNet++ inference time [ms]	0	56	56	0	0	56	56
Source rate [Mbps]	256.3	120.9	18.8	5.7	16.2	8	1.3
Throughput ($d < 50$ m) [Mbps]	259.4	124.3	20.2	5.6	17.3	8.6	1.4
Throughput ($d > 50$ m) [Mbps]	151	72.2	11.3	2.9	10	5	0.7

Fig. 6: Mean throughput and confidence intervals (shaded areas) vs. d , and for different HSC compression configurations. Solid (dashed) lines are relative to the use of real data from SemanticKITTI (statistical traffic models).Fig. 7: Mean latency and confidence intervals (shaded areas) vs. d , and for different HSC compression configurations. Solid (dashed) lines are relative to the use of real data from SemanticKITTI (statistical traffic models).

high (around 50 dB), as the channel is mainly in Line of Sight (LoS) conditions. As the vehicle moves away from the gNB, the LoS probability (green line) decreases according to the model in [62], and the SINR drops down to -12 dB at 300 m. This translates into a slow degradation of the theoretical capacity of the channel that, considering the average (25% quantile) SINR, varies between 3.14 (3) Gbps, 2.75 (1.63) Gbps, and 16.42 (1.8) Mbps at 15, 45, and 300 m, respectively. These results are also confirmed by the Packet Receipt Rate (PRR) reported in Table V, which decreases as d increases. For $d < 45$ m, all the packets are successfully delivered; however, as $d > 45$ m, the packet loss increases due to the worse channel conditions.

2) *Throughput and latency*: Table VI reports the average source rate of the application, calculated by multiplying the

average data size by the rate of the LiDAR (10 Hz).⁴ The results indicate that existing V2X technologies cannot support the source rate of raw data (256.3 Mbps for D0/S0) or when conservative compression is applied (e.g., 120.9 Mbps for D0/S1). For comparison, the peak nominal throughput of the IEEE 802.1p protocol is only 27 Mbps [63], which motivates the need for compression and/or more advanced V2X solutions like NR V2X operating at mmWaves [9].

In Figs. 6 and 7 we plot the E2E throughput and latency, respectively, vs. d . The dashed lines are for the results obtained using real data from SemanticKITTI, while solid lines correspond to using statistical traffic models. We clearly see that there is an almost perfect overlap between the two sets of curves for all HSC compression configurations and values of d . We conclude that replacing real data with statistical traffic models has a negligible impact on the network. Interestingly, this is true also for model D0/S0, that did not pass the KS test in Sec. IV-B; although this model is not formally accurate to characterize the size of LiDAR data, it remains sufficiently precise in terms of network metrics.

Moreover, we see that the throughput (latency) decreases (increases) as d increases, which is due to the lower SINR at long distance. From Fig. 7, we see that the latency is always below the application requirement for autonomous driving (set to 100 ms based on 3GPP specifications [21]) for all compression configurations except D0/S1 and when $d > 100$ m. This may seem counterintuitive, considering that

⁴Note that, unlike the throughput, the source rate does not include the headers nor the communication overhead introduced by the protocol stack. This explains why the throughput can be slightly larger than the source rate in some cases (e.g., D0/S2, D14/S0–2).

d [m]	D0/S0	D0/S1	D0/S2	D11/S0	D14/S0	D14/S1	D14/S2
15	✓	✓	✓	✓	✓	✓	✓
30	✓	✓	✓	✓	✓	✓	✓
45	✓	✓	✓	✓	✓	✓	✓
60	✓	✓	✓	✓	✓	✓	✓
75	✓	✓	✓	✓	✓	✓	✓
90	✓	✓	✓	✓	✓	✓	✓
105	✓	✓	✓	✓	✓	✓	✓
120	✓	✓	✓	✓	✓	✓	✓
135	✓	✓	✓	✓	✓	✓	✓
165	✗	✓	✓	✓	✓	✓	✓
195	✗	✓	✓	✓	✓	✓	✓
225	✗	✓	✓	✓	✓	✓	✓
255	✗	✓	✓	✓	✓	✓	✓
285	✓	✓	✓	✓	✓	✓	✓
300	✗	✓	✓	✓	✓	✓	✓

TABLE VII: Results of the KS test for the E2E throughput obtained using the statistical models and real data with the SemanticKITTI dataset. The mark ✓(✗) is used if the test is passed (not passed).

d [m]	D0/S0	D0/S1	D0/S2	D11/S0	D14/S0	D14/S1	D14/S2
15	✓	✓	✓	✓	✓	✓	✓
30	✓	✓	✓	✓	✓	✓	✓
45	✓	✓	✓	✓	✓	✓	✓
60	✓	✓	✓	✓	✓	✓	✓
75	✓	✓	✓	✓	✓	✓	✓
90	✓	✓	✓	✓	✓	✓	✓
105	✓	✓	✓	✓	✓	✓	✓
120	✓	✓	✓	✓	✓	✓	✓
135	✓	✓	✓	✓	✓	✓	✓
165	✓	✓	✓	✗	✓	✗	✗
195	✓	✓	✓	✓	✓	✓	✓
225	✓	✓	✓	✓	✗	✓	✓
255	✓	✓	✓	✓	✗	✓	✓
285	✓	✓	✓	✓	✓	✓	✓
300	✓	✓	✓	✓	✓	✓	✓

TABLE VIII: Results of the KS test for the E2E latency obtained using the statistical models and real data with the SemanticKITTI dataset. The mark ✓(✗) is used if the test is passed (not passed).

D0/S1 applies more compression than D0/S0 (raw data), so data transmission should be faster in principle. However, for D0/S1, the additional inference time of RangeNet++ (i.e., 56 ms as reported in Table VI), combined with the encoding and decoding times for compression, must also be considered, which is not the case for D0/S0. The performance further improves for D11/S0, suggesting that reducing the number of quantization bits is desirable for both throughput and latency. Conversely, increasing the SL from S0 to S1 and S2 improves the throughput, at the cost of latency, again due to the additional inference time required for segmentation. Nevertheless, at short distance, the latency remains under the 100 ms threshold.

Finally, notice that a more aggressive compression configuration might inevitably degrade the quality of the point cloud (generally measured in terms of the mean Average Precision (mAP)), and affect the performance of object detection algorithms at the receiver. This analysis was partially addressed in [64], [65], and is out of the scope of this paper.

3) *Model accuracy*: We now formally validate the accuracy of the statistical models for the file size of the point clouds derived in Sec. IV measuring their impact on network metrics. To do so, we repeat the KS test on the E2E throughput and latency. The results are reported in Tables VII and VIII, respectively. As expected, the test is passed for almost all compression configurations and distances, so it is another demonstration of the accuracy of the selected models. The

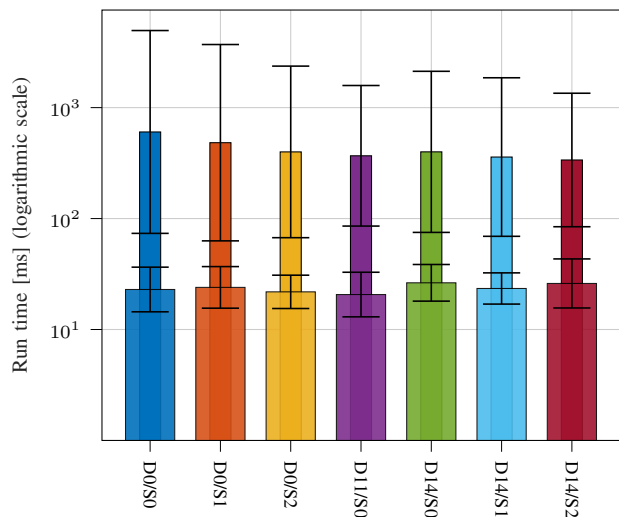


Fig. 8: Average run time for different HSC compression configurations measured in ns-3 on real data from the SemanticKITTI dataset (narrow bars) and using the statistical traffic models (wide bars).

only exception is with D0/S0, which also failed the test in Sec. IV-B, and for $d > 150$ m, where propagation is largely in non-Line-of-Sight (nLoS). In this range, the channel is severely unstable and may introduce unpredictable non-linear behaviors, making the statistical models less representative of the real data.

4) *Run time*: Finally, in Fig. 8 we report the run time of a single simulations run in ns-3 using either the *BurstyApplication*, i.e., real data from the SemanticKITTI dataset (narrow bars), or the *StatisticalTraffic* application, which relies on statistical models (wide bars). As expected, the run time improves when using statistical models, with an average speed-up factor of 18 \times . The maximum gain is observed with raw data (D0/S0), where the simulation time decreases from over 10 minutes to approximately 22 seconds (26 \times speed-up).

In conclusion, the *StatisticalTraffic* application proves to be a valid alternative to the *BurstyApplication*, delivering substantial improvements in simulation run time while maintaining high accuracy. The only restriction is for $d > 150$ m, where our statistical models may not fully capture the characteristics of real data. However, this limitation is negligible since direct V2X communication at these distances is generally impractical, if not entirely infeasible, under realistic latency constraints.

VII. CONCLUSION

In this paper we proposed a comprehensive statistical characterization for the size of LiDAR point clouds based on the SemanticKITTI dataset, to be used for network simulations in an automotive driving scenario. We obtained seven distinct distributions to model raw data and six representative compression configurations using the state-of-the-art HSC algorithm. The statistical models have been rigorously validated through a Kolmogorov-Smirnov test with Bootstrap Resampling, with the exception of the model representing raw (uncompressed) data that did not pass the test. Furthermore, we implemented these random distributions in ns-3, and ran a simulation campaign to evaluate their accuracy in terms of some E2E network metrics. Our results showed a perfect match between our

statistical traffic models and real data from SemanticKITTI. We also observed that compression can significantly improve the network throughput, and highlighted the critical trade-off between compression ratio and latency. Additionally, we found that using statistical models substantially improves the simulation run time compared to using real data, while maintaining high accuracy. However, the reliability decreases for distances beyond 150 m, where channel conditions become statistically unstable.

As part of future work, we will leverage the flexibility of HSC to further refine our models, incorporating additional factors such as the impact of compression on data quality and energy consumption, besides performance metrics such as throughput and latency.

REFERENCES

- [1] M. Giordani, M. Polese, M. Mezzavilla, S. Rangan, and M. Zorzi, "Toward 6G Networks: Use Cases and Technologies," *IEEE Commun. Mag.*, vol. 58, no. 3, pp. 55–61, March 2020.
- [2] D. J. Fagnant and K. Kockelman, "Preparing a nation for autonomous vehicles: opportunities, barriers and policy recommendations," *Transportation Research Part A: Policy and Practice*, vol. 77, pp. 167–181, Jul. 2015.
- [3] N. Lu, N. Cheng, N. Zhang, X. Shen, and J. W. Mark, "Connected vehicles: Solutions and challenges," *IEEE Internet of Things Journal*, vol. 1, no. 4, pp. 289–299, Aug. 2014.
- [4] Y. Li and J. Ibanez-Guzman, "LiDAR for autonomous driving: The principles, challenges, and trends for automotive LiDAR and perception systems," *IEEE Signal Processing Magazine*, vol. 37, no. 4, pp. 50–61, Jul. 2020.
- [5] D. Feng, C. Haase-Schütz, L. Rosenbaum, H. Hertlein, C. Glaeser, F. Timm, W. Wiesbeck, and K. Dietmayer, "Deep multi-modal object detection and semantic segmentation for autonomous driving: Datasets, methods, and challenges," *IEEE Transactions on Intelligent Transportation Systems*, vol. 22, no. 3, pp. 1341–1360, Mar. 2020.
- [6] L. Hobert, A. Festag, I. Llatser, L. Altomare, F. Visintainer, and A. Kovacs, "Enhancements of V2X communication in support of cooperative autonomous driving," *IEEE Communications Magazine*, vol. 53, no. 12, pp. 64–70, Dec. 2015.
- [7] T. Higuchi, M. Giordani, A. Zanella, M. Zorzi, and O. Altintas, "Value-anticipating V2V communications for cooperative perception," in *IEEE Intelligent Vehicles Symposium (IV)*, Jun. 2019.
- [8] P. Testolina, F. Barbato, U. Michieli, M. Giordani, P. Zanuttigh, and M. Zorzi, "SELMMA: SEmantic Large-Scale Multimodal Acquisitions in Variable Weather, Daytime and Viewpoints," *IEEE Transactions on Intelligent Transportation Systems*, vol. 24, no. 7, pp. 7012–7024, Jul. 2023.
- [9] T. Zugno, M. Drago, M. Giordani, M. Polese, and M. Zorzi, "Toward Standardization of Millimeter-Wave Vehicle-to-Vehicle Networks: Open Challenges and Performance Evaluation," *IEEE Communications Magazine*, vol. 58, no. 9, pp. 79–85, Sep. 2020.
- [10] F. Nardo, D. Peressoni, P. Testolina, M. Giordani, and A. Zanella, "Point cloud compression for efficient data broadcasting: A performance comparison," in *IEEE Wireless Communications and Networking Conference (WCNC)*, 2022.
- [11] J. Behley, M. Garbade, A. Milioto, J. Quenzel, S. Behnke, C. Stachniss, and J. Gall, "SemanticKITTI: A dataset for semantic scene understanding of LiDAR sequences," in *Proceedings of the IEEE/CVF International Conference on Computer Vision*, 2019, pp. 9297–9307.
- [12] D. Graziosi, O. Nakagami, S. Kuma, A. Zagherro, T. Suzuki, and A. Tabatabai, "An overview of ongoing point cloud compression standardization activities: Video-based (V-PCC) and geometry-based (G-PCC)," *APSIPA Transactions on Signal and Information Processing*, vol. 9, p. e13, Apr. 2020.
- [13] M. Lecci, P. Testolina, M. Polese, M. Giordani, and M. Zorzi, "Accuracy versus complexity for mmWave ray-tracing: A full stack perspective," *IEEE Transactions on Wireless Communications*, vol. 20, no. 12, pp. 7826–7841, Dec. 2021.
- [14] J. Cao, W. S. Cleveland, Y. Gao, K. Jeffay, F. D. Smith, and M. Weigle, "Stochastic models for generating synthetic HTTP source traffic," in *IEEE Conference on Computer Communications (INFOCOM)*, 2004.
- [15] M. Lecci, A. Zanella, and M. Zorzi, "An ns-3 implementation of a bursty traffic framework for virtual reality sources," in *ACM Workshop on Ns-3*, 2021.
- [16] W. Buller, B. Wilson, L. van Nieuwstadt, and J. Ebling, "Statistical modelling of measured automotive radar reflections," in *IEEE International Instrumentation and Measurement Technology Conference (I2MTC)*, 2013.
- [17] M. Ahmadi-Pour, T. Ludwig, and C. Olaverri-Monreal, "Statistical modelling of multi-sensor data fusion," in *IEEE International Conference on Vehicular Electronics and Safety (ICVES)*, 2017.
- [18] A. Varischio, F. Mandruzzato, M. Bullo, M. Giordani, P. Testolina, and M. Zorzi, "Hybrid Point Cloud Semantic Compression for Automotive Sensors: A Performance Evaluation," in *IEEE International Conference on Communications (ICC)*, 2021.
- [19] C. Wang, B. Zeng, and J. Shao, "Application of bootstrap method in Kolmogorov-Smirnov test," in *International Conference on Quality, Reliability, Risk, Maintenance, and Safety Engineering*, 2011.
- [20] J. Choi, V. Va, N. Gonzalez-Prelcic, R. Daniels, C. R. Bhat, and R. W. Heath, "Millimeter-wave vehicular communication to support massive automotive sensing," *IEEE Communications Magazine*, vol. 54, no. 12, pp. 160–167, Dec. 2016.
- [21] 3GPP, "Service requirements for enhanced V2X scenarios," Technical Specifications (TS) 22.186, Apr. 2022, version 17.0.0.
- [22] L. Huo, D. Jiang, X. Zhu, Y. Wang, Z. Lv, and S. Singh, "A SDN-based fine-grained measurement and modeling approach to vehicular communication network traffic," *International Journal of Communication Systems*, vol. 35, no. 12, p. e4092, Jul. 2022.
- [23] J. Zerwas, K. Aykurt, S. Schmid, and A. Blenk, "Network traffic characteristics of machine learning frameworks under the microscope," in *17th International Conference on Network and Service Management (CNSM)*, 2021.
- [24] J. Navarro-Ortiz, P. Romero-Diaz, S. Sendra, P. Ameigeiras, J. J. Ramos-Munoz, and J. M. Lopez-Soler, "A Survey on 5G Usage Scenarios and Traffic Models," *IEEE Communications Surveys & Tutorials*, vol. 22, no. 2, pp. 905–929, Secondquarter 2020.
- [25] A. Bulashenko, S. Piltyay, A. Polishchuk, and O. Bulashenko, "New Traffic Model of M2M Technology in 5G Wireless Sensor Networks," in *IEEE 2nd International Conference on Advanced Trends in Information Theory (ATIT)*, 2020.
- [26] O. N. Østerbø, D. Zucchetto, K. Mahmood, A. Zanella, and O. Grøndalen, "State modulated traffic models for machine type communications," in *International Teletraffic Congress (ITC 29)*, 2017.
- [27] M. Sansoni, G. Ravagnani, D. Zucchetto, C. Pielli, A. Zanella, and K. Mahmood, "Comparison of M2M traffic models against real world data sets," in *IEEE 23rd International Workshop on Computer Aided Modeling and Design of Communication Links and Networks (CAMAD)*, 2018.
- [28] L. Lao, Z. Li, S. Hou, B. Xiao, S. Guo, and Y. Yang, "A Survey of IoT Applications in Blockchain Systems: Architecture, Consensus, and Traffic Modeling," *ACM Comput. Surv.*, vol. 53, no. 1, Feb. 2020.
- [29] S. Tanwir and H. Perros, "A survey of VBR video traffic models," *IEEE Communications Surveys & Tutorials*, vol. 15, no. 4, pp. 1778–1802, Fourthquarter 2013.
- [30] H. Kalbkhani, M. G. Shayesteh, and N. Haghight, "Adaptive LSTAR Model for Long-Range Variable Bit Rate Video Traffic Prediction," *IEEE Transactions on Multimedia*, vol. 19, no. 5, pp. 999–1014, May 2017.
- [31] M. Lecci, F. Chiariotti, M. Drago, A. Zanella, and M. Zorzi, "Temporal characterization of XR traffic with application to predictive network slicing," in *IEEE 23rd International Symposium on a World of Wireless, Mobile and Multimedia Networks (WoWMoM)*, 2022.
- [32] F. Chiariotti, M. Drago, P. Testolina, M. Lecci, A. Zanella, and M. Zorzi, "Temporal characterization and prediction of VR traffic: A network slicing use case," *IEEE Transactions on Mobile Computing*, vol. 23, no. 5, pp. 3890–3908, May 2023.
- [33] E. Grigoreva, M. Laurer, M. Vilgelm, T. Gehrsitz, and W. Kellerer, "Coupled Markovian Arrival Process for Automotive Machine Type Communication traffic modeling," in *IEEE International Conference on Communications (ICC)*, 2017.
- [34] L. Nie, X. Wang, L. Wan, S. Yu, H. Song, D. Jiang, and K. Zhang, "Network Traffic Prediction Based on Deep Belief Network and Spatiotemporal Compressive Sensing in Wireless Mesh Backbone Networks," *Wirel. Commun. Mob. Comput.*, vol. 2018, Jan. 2018.
- [35] Q. Zhuo, Q. Li, H. Yan, and Y. Qi, "Long short-term memory neural network for network traffic prediction," in *12th International Conference on Intelligent Systems and Knowledge Engineering (ISKE)*, 2017.

- [36] L. Zhang, H. Zhang, Q. Tang, P. Dong, Z. Zhao, Y. Wei, J. Mei, and K. Xue, "LNTP: An End-to-End Online Prediction Model for Network Traffic," *IEEE Network*, vol. 35, no. 1, pp. 226–233, Jan./Feb. 2021.
- [37] C.-H. Wang, T. Shimizu, H. Muralidharan, and A. Yamamuro, "A Real-Time High-Definition Vehicular Sensor Data Sharing System using Millimeter Wave V2V Communications," in *IEEE Vehicular Networking Conference (VNC)*, 2020.
- [38] Q. Chen, S. Tang, J. Hochstetler, J. Guo, Y. Li, J. Xiong, Q. Yang, and S. Fu, "Low-latency high-level data sharing for connected and autonomous vehicular networks," in *IEEE International Conference on Industrial Internet (ICII)*, 2019.
- [39] A. Milioto, I. Vizzo, J. Behley, and C. Stachniss, "RangeNet ++: Fast and Accurate LiDAR Semantic Segmentation," in *IEEE/RSJ International Conference on Intelligent Robots and Systems (IROS)*, 2019.
- [40] Google, "Draco 3D Data Compression," 2017, [Online]. Available: <https://github.com/google/draco>.
- [41] L. Wang, Y. Huang, Y. Hou, S. Zhang, and J. Shan, "Graph Attention Convolution for Point Cloud Semantic Segmentation," in *Proceedings of the IEEE/CVF Conference on Computer Vision and Pattern Recognition (CVPR)*, June 2019.
- [42] L. Tchammi, C. Choy, I. Armeni, J. Gwak, and S. Savarese, "SEGCloud: Semantic Segmentation of 3D Point Clouds," in *International Conference on 3D Vision (3DV)*, 2017.
- [43] Y. Zhang, Y. Qu, Y. Xie, Z. Li, S. Zheng, and C. Li, "Perturbed Self-Distillation: Weakly Supervised Large-Scale Point Cloud Semantic Segmentation," in *Proceedings of the IEEE/CVF International Conference on Computer Vision (ICCV)*, 2021.
- [44] Y. Zhang, Z. Zhou, P. David, X. Yue, Z. Xi, B. Gong, and H. Foroosh, "PolarNet: An Improved Grid Representation for Online LiDAR Point Clouds Semantic Segmentation," in *Proceedings of the IEEE/CVF Conference on Computer Vision and Pattern Recognition (CVPR)*, 2020.
- [45] B. Wu, X. Zhou, S. Zhao, X. Yue, and K. Keutzer, "SqueezeSegV2: Improved Model Structure and Unsupervised Domain Adaptation for Road-Object Segmentation from a LiDAR Point Cloud," in *International Conference on Robotics and Automation (ICRA)*, 2019.
- [46] W. Lau, Z. Li, and K. W. Lam, "Effects of JPEG compression on image classification," *International Journal of Remote Sensing*, vol. 24, no. 7, pp. 1535–1544, Jun. 2003.
- [47] T. Gandor and J. Nalepa, "First Gradually, Then Suddenly: Understanding the Impact of Image Compression on Object Detection Using Deep Learning," *Sensors*, vol. 22, no. 3, Feb. 2022.
- [48] Y.-Y. Jo, Y. S. Choi, H. W. Park, J. H. Lee, H. Jung, H.-E. Kim, K. Ko, C. W. Lee, H. S. Cha, and Y. Hwangbo, "Impact of image compression on deep learning-based mammogram classification," *Scientific Reports*, vol. 11, no. 1, p. 7924, Apr 2021.
- [49] D. Tian, H. Ochimizu, C. Feng, R. Cohen, and A. Vetro, "Geometric distortion metrics for point cloud compression," in *IEEE International Conference on Image Processing (ICIP)*, 2017.
- [50] F. J. Massey Jr, "The Kolmogorov-Smirnov test for goodness of fit," *Journal of the American statistical Association*, vol. 46, no. 253, pp. 68–78, Apr. 1951.
- [51] G. J. Babu and C. R. Rao, "Goodness-of-fit tests when parameters are estimated," *Sankhyā: The Indian Journal of Statistics*, vol. 66, no. 1, pp. 63–74, Jan. 2004.
- [52] G. Babu and E. Feigelson, "Astrostatistics: Goodness-of-fit and all that!" in *Astronomical Data Analysis Software and Systems XV*, vol. 351, 2006, p. 127.
- [53] T. R. Henderson, M. Lacage, G. F. Riley, C. Dowell, and J. Kopena, "Network simulations with the ns-3 simulator," *SIGCOMM*, 2008.
- [54] M. Drago, T. Zugno, M. Polese, M. Giordani, and M. Zorzi, "MilliCar: An ns-3 module for mmWave NR V2X networks," in *Workshop on ns-3*, 2020.
- [55] D. Krajzewicz, J. Erdmann, M. Behrisch, and L. Bieker, "Recent development and applications of SUMO-Simulation of Urban MObility," *International journal on advances in systems and measurements*, vol. 5, no. 3&4, Dec. 2012.
- [56] M. Drago, T. Zugno, F. Mason, M. Giordani, M. Boban, and M. Zorzi, "Artificial Intelligence in Vehicular Wireless Networks: A Case Study Using ns-3," in *ACM Workshop on Ns-3*, 2022.
- [57] M. Lecci, M. Drago, A. Zanella, and M. Zorzi, "An Open Framework for Analyzing and Modeling XR Network Traffic," *IEEE Access*, vol. 9, pp. 129 782–129 795, Sep. 2021.
- [58] M. Mezzavilla, M. Zhang, M. Polese, R. Ford, S. Dutta, S. Rangan, and M. Zorzi, "End-to-end simulation of 5g mmwave networks," *IEEE Communications Surveys & Tutorials*, vol. 20, no. 3, pp. 2237–2263, April 2018.
- [59] G. Piro, N. Baldo, and M. Miozzo, "An LTE module for the ns-3 network simulator," in *Proceedings of the 4th International Conference on Simulation Tools and Techniques*, 2011.
- [60] W. T. Shaw, "Sampling Student's T distribution-use of the inverse cumulative distribution function," *Journal of Computational Finance*, vol. 9, no. 4, p. 37, Jan. 2006.
- [61] J.-Y. L. Boudec, *Performance Evaluation of Computer and Communication Systems*. EFPL Press, 2011.
- [62] 3GPP, "Study on channel model for frequencies from 0.5 to 100 GHz," Technical Report (TR) 38.901, 2018.
- [63] K. Abboud, H. A. Omar, and W. Zhuang, "Interworking of DSRC and Cellular Network Technologies for V2X Communications: A Survey," *IEEE Transactions on Vehicular Technology*, vol. 65, no. 12, pp. 9457–9470, Dec. 2016.
- [64] F. Mason, M. Drago, T. Zugno, M. Giordani, M. Boban, and M. Zorzi, "A reinforcement learning framework for PQoS in a teleoperated driving scenario," in *IEEE Wireless Communications and Networking Conference (WCNC)*, 2022.
- [65] F. Bragato, M. Giordani, and M. Zorzi, "Federated Reinforcement Learning to Optimize Teleoperated Driving Networks," in *IEEE Global Communications Conference*, 2022. [Online]. Available: <https://arxiv.org/abs/2410.02312>